

Alma Mater Studiorum Università di Bologna
Archivio istituzionale della ricerca

Discovery of cryptotephra at Middle-Upper Paleolithic sites Arma Veirana and Riparo Bombrini, Italy: a new link for broader geographic correlations

This is the final peer-reviewed author's accepted manuscript (postprint) of the following publication:

Published Version:

Hirniak, J.N., Smith, E.I., Johnsen, R., Ren, M., Hodgkins, J., Orr, C., et al. (2020). Discovery of cryptotephra at Middle-Upper Paleolithic sites Arma Veirana and Riparo Bombrini, Italy: a new link for broader geographic correlations. JOURNAL OF QUATERNARY SCIENCE, 35(1-2), 199-212 [10.1002/jqs.3158].

Availability:

This version is available at: <https://hdl.handle.net/11585/706361> since: 2019-11-27

Published:

DOI: <http://doi.org/10.1002/jqs.3158>

Terms of use:

Some rights reserved. The terms and conditions for the reuse of this version of the manuscript are specified in the publishing policy. For all terms of use and more information see the publisher's website.

This item was downloaded from IRIS Università di Bologna (<https://cris.unibo.it/>).
When citing, please refer to the published version.

(Article begins on next page)

This is the peer reviewed version of the following article:

Hirniak JN, Smith E, Johnsen R, Ren M, Hodgkins J, Orr C, Negrino F, Riel-Salvatore J, Fitch S, Miller CE, Zerboni A, Mariani GS, Harris J, Gravel-Miguel C, Strait D, Peresani M, **Benazzi S**, Marean CW, 2019. Discovery of cryptotephra at Middle-Upper Paleolithic sites Arma Veirana and Riparo Bombrini, Italy: A new link for broader geographic correlations. *Journal of Quaternary Science*, 1-14 (Online Early View)

which has been published in final form at <https://doi.org/10.1002/jqs.3158>

This article may be used for non-commercial purposes in accordance with Wiley Terms and Conditions for Use of Self-Archived Versions.

Discovery of cryptotephra at Middle–Upper Paleolithic sites Arma Veirana and Riparo Bombrini, Italy: a new link for broader geographic correlations

JAYDE N. HIRNIAK,^{1*} EUGENE I. SMITH,² RACHEAL JOHNSEN,² MINGHUA REN,² JAMIE HODGKINS,³ CALEY ORR,^{3,4} FABIO NEGRINO,⁵ JULIEN RIEL-SALVATORE,⁶ SHELBY FITCH,² CHRISTOPHER E. MILLER,⁷ ANDREA ZERBONI,⁸ GUIDO S. MARIANI,⁹ JACOB A. HARRIS,¹ CLAUDINE GRAVEL-MIGUEL,¹ DAVID STRAIT,^{10,11} MARCO PERESANI,¹² STEFANO BENAZZI¹³ and CURTIS W. MAREAN^{1,14}

¹Institute of Human Origins, School of Human Evolution and Social Change, Arizona State University, PO Box 874101, Tempe, AZ, 85287-4101, USA

²Department of Geoscience, University of Nevada Las Vegas, 4505 Maryland Parkway, Las Vegas, NV, 89154, USA

³Department of Anthropology, University of Colorado Denver, 1200 Larimer Street, Denver, CO, 80217-3364, USA

⁴Department of Cell and Developmental Biology, University of Colorado School of Medicine, Mail Stop F435, 13001 17th Place, Aurora, CO, 80045, USA

⁵Dipartimento di Antichità, Filosofia e Storia (DAFIST), Università di Genova (Italy), Via Balbi 2, Genoa, 16126, Italy

⁶Département d'Anthropologie Université de Montréal, Pavillon Lionel-Groulx, 3150 Rue Jean-Brillant, Montréal, QC, H3T 1N8, Canada

⁷Institute for Archaeological Sciences and Senckenberg Centre for Human Evolution and Paleoenvironment, University of Tübingen, Rümelinstr. 23, Tübingen, 72070, Germany

⁸Dipartimento di Scienze Della Terra 'A. Desio', Università Degli Studi di Milano, Via L. Mangiagalli 34, 20133, Milano, Italy

⁹Università Degli Studi di Cagliari, Cittadella Universitaria di Monserrato, Monserrato, 09042, (CA), Italy

¹⁰Department of Anthropology, Washington University in St Louis, One Brookings Drive, Campus Box 1114, St Louis, MO, 63130, USA

¹¹Palaeo-Research Institute, University of Johannesburg, Auckland Park, Gauteng, South Africa

¹²Section of Prehistoric and Anthropological Science, Department of Humanities, University of Ferrara, Ferrara, I-44100, Italy

¹³Department of Cultural Heritage, University of Bologna, Ravenna, 48121, Italy

¹⁴African Centre for Coastal Palaeoscience, Nelson Mandela University, Port Elizabeth, Eastern Cape, 6031, South Africa

ABSTRACT: Chemical characterization of cryptotephra is critical for temporally linking archaeological sites. Here, we describe cryptotephra investigations of two Middle–Upper Paleolithic sites from north-west Italy, Arma Veirana and Riparo Bombrini. Cryptotephra are present as small (<100 µm) rhyolitic glass shards at both sites, with geochemical signatures rare for volcanoes in the Mediterranean region. Two chemically distinct shard populations are present at Arma Veirana (P1 and P2). P1 is a high silica rhyolite (>75 wt.%) with low FeO (<1 wt.%) and a K₂O/Na₂O > 1 and P2 is also a high silica rhyolite (>75 wt.%) but with higher FeO (2.33–2.65 wt.%). Shards at Riparo Bombrini (P3) are of the same composition as P1 shards at Arma Veirana, providing a distinct link between deposits at both sites. Geochemical characteristics suggest three possible sources for P1 and P3: eruptions from Lipari Island (56–37.7 ka) in Italy, the Acigöl volcanic field (200–20 ka) in Turkey and the Miocene Kirka-Phrigan caldera (18 Ma) in Turkey. Eruptions from Lipari Island are the most likely source for P1,3 cryptotephra. This study highlights how cryptotephra can benefit archaeology, by providing a direct link between Arma Veirana and Riparo Bombrini as well as other deposits throughout the Mediterranean.

KEYWORDS: cryptotephra; Middle Paleolithic; radiocarbon dating; tephrochronology; Upper Paleolithic.

Introduction

Tephrochronology has long been a critical correlative tool in geology, paleoecology and paleoanthropology (Ewart, 1963; Sarna-Wojcicki *et al.*, 1985; Lowe, 1990, 2011; Feibel, 1999). Long-distance correlations of tephra have been useful for understanding the eruptive history of a volcano, which is key for hazard prediction (Shane and Hovard, 2002; Gehrels *et al.*, 2006). However, the use of tephrochronology has also aided in better understanding early hominin evolution (Brown *et al.*, 1985) as well as reconstructing paleoenvironmental contexts (Feibel *et al.*, 1989). To provide a precise chronological marker, tephra must be sourced to a volcanic eruption whose age is known from independent dating methods. Unlike other material, tephra can provide a marker horizon even without a calculated age due to the specific geochemical signatures associated with each eruption (Feibel, 1999; Lowe, 2011; Lane *et al.*, 2014). This allows scientists to link stratigraphic sequences across large regions without knowing the exact source eruption, through methods of tephrostratigraphy (Feibel, 1999), further demonstrating the wide applicability of this approach.

Within the last two decades, tephrochronology has become more common in archaeological research due to advancements in extraction and identification methods (Blockley *et al.*, 2005) and due to its ability to work as a correlative tool as well as to more accurately date deposits (Riede and Thastrup, 2013; Douka *et al.*, 2014; Lowe *et al.*, 2015; Smith *et al.*, 2018). While the basic approach is similar to correlative studies that have been conducted as far back as the early 1950s (Lowe, 1990), the use of cryptotephra (microscopic volcanic glass shards) in archaeological research has shown great success for large-scale correlations (Lowe *et al.*, 2015). Cryptotephra preserves well in a variety of depositional environments (e.g. peat bogs, marine and lake sediments, ice cores) and can travel as far as 9000 km from the source eruption (Smith *et al.*, 2018), allowing for isochrons (precise temporal markers) to be established between archaeological and paleoenvironmental records across vast regions (Lane *et al.*, 2014; Lowe *et al.*, 2015). However, the ability to find, recognize and analyze cryptotephra involves specialized extraction methods that target the non-visible shards (Blockley *et al.*, 2005; Lane *et al.*, 2014), making it possible to locate these microscopic shards even at very low quantities (Smith *et al.*, 2018). The extraction of shards from host sediments can be very difficult and even when shards are identified, using them as stratigraphic markers can be problematic. The identified shards must show signs of minimal reworking to be a reliable stratigraphic and temporal marker (Lane *et al.*, 2014). If shards have been severely reworked, then the location is not indicative of primary deposition and therefore cannot be used as a reliable marker horizon. Fortunately, with an understanding of site formation processes at a particular site, these issues can be resolved. Historically, cryptotephra studies have been critical for correlating sedimentary deposits and understanding the dynamics of past volcanic eruptions. Today, they are also extremely important in the field of archaeology for independently testing age models derived from other techniques (Douka *et al.*, 2014; Smith *et al.*, 2018), linking archaeological deposits (Barton *et al.*, 2015; Lowe *et al.*, 2015;

Smith *et al.*, 2018), and assisting with dating sites older than the limit of radiocarbon dating (Veres *et al.*, 2018).

This contribution presents the results of cryptotephra investigations at two Middle–Upper Paleolithic sites, Arma Veirana (AV) and Riparo Bombrini (RB), located in Liguria, Italy. The sites are 80 km apart and contain similar Middle–Upper Paleolithic archaeological assemblages; however, dating the Middle Paleolithic deposits at both sites has been difficult. At AV, current radiocarbon dates for the Mousterian-bearing strata have so far been inconclusive, but they range from near the limit of radiocarbon dating to beyond the limits (possibly > 50 ka; J. Hodgkins, 2019, unpublished data). At RB, there are radiocarbon dates near the dating limit as well as some dating inversions (Holt *et al.*, 2019). Therefore, for this study, we sampled the two sites in the hope of finding shards of similar composition. This would allow us to better date the assemblages, provided the shards could be correlated to a radiometrically dated eruption. Additionally, cryptotephra can assist in correlating the occupational history of both sites and establish an isochron applicable to other Paleolithic sites in southern Europe. Here, we report shard compositions and discuss the stratigraphic locations of shards at both sites based on a shard count profile and micromorphological analyses. These analyses are important to understand the depositional processes that may have affected the shards and to identify a reliable isochron. These results highlight the benefits of cryptotephra correlations as well as important factors that must be considered when using this tool on archaeological sites.

Site description

Arma Veirana (AV)

AV is a limestone cave situated on the south side of Neva Valley in Liguria (44°08'45.4"N, 08°04'18.8"E) approximately 14 km from the Mediterranean coast (Fig. 1). It formed through differential erosion along a fault and is carved into a north-facing cliff. The cave floor slopes upward to the south, exposing younger sediments in the back and older sediments near the mouth of the cave. Formal excavations at AV began in 2015. *In situ* Middle and Upper Paleolithic deposits were excavated in trenches located near the mouth of the site, suggesting that most of the deposits are undisturbed. Micromorphological analyses show that bioturbation is present at AV; however, the amount of reworking between distinct stratigraphic units is minimal and limited to a few centimeters at the contacts. This is important for identifying the exact stratigraphic location of shards (see 'Distinguishing primary and re-worked tephra' for a detailed discussion).

The stratigraphic units uncovered in the main trenches are, from bottom to top, Black Mousterian (BM), Granular (Gr), Compact Strong Brown (CSB) and Rocky Brown (RB). The CSB, Gr, and BM have yielded Mousterian lithics. Each stratigraphic unit contains a mixture of material and is likely to have accumulated by colluviation and roof-fall. The BM fine fraction consists of sandy, clayey silt with sub-rounded, gravel-sized fragments of bedrock. It is dark grayish brown (10YR 3/2) which is clearly derived from the abundance of anthropogenic components (charcoal, bone fragments, burned bone) (Fig. 2). The Gr is dominated by a medium sandy silt that contains granules and gravel throughout. It contains a granular microstructure and is less compact than the BM. Packing voids are present, but anthropogenic components are rare (Fig. 2). The proportion of comminuted charcoal and other combustion residues decrease noticeably as one moves upward in the section, which suggests less anthropogenic influence.

Radiocarbon dating of the Mousterian-bearing deposits at AV produced inconsistent results. Oxford University and Eidgenössische Technische Hochschule (ETH) Zürich analyzed charcoal and bone samples collected on site. Analyses at ETH Zürich dated the BM to 43 781–43 121 cal a BP and the Gr to 41 721–41 174 cal a BP. Calibration for samples were performed using OxCal 4.2 (Bronk Ramsey, 2013) and the IntCal13 calibration dataset (Reimer *et al.*, 2013). Samples were analyzed again at Oxford University and resulted in infinite ages (>45 000 ¹⁴C a BP) except one charcoal sample in stratigraphic unit Gr (49 400 ± 1900 ¹⁴C a BP; J. Hodgkins, 2019, unpublished data). It is possible these variations are due to samples being processed at different laboratories; however, the results remain inconsistent. Therefore, the age of the Middle Paleolithic occupation at AV remains inconclusive.

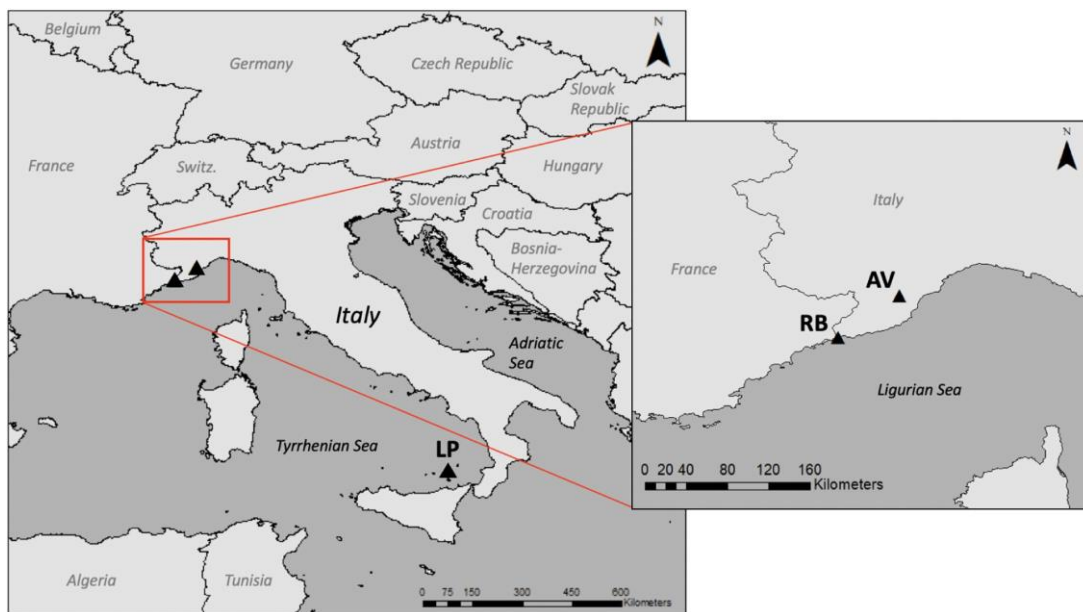


Figure 1. Location of study sites. AV is Arma Veirana located in the Ligurian pre-Alps. RB is Riparo Bombrini located at the Franco-Italian border, along the present-day coastline. LP is Lipari Island and is the location of a potential source volcano.

Riparo Bombrini (RB)

RB is a collapsed rock shelter located on the Mediterranean coast near the Franco-Italian border (43°46'59.6"N, 07°32' 7.6"E) (Fig. 1). The site was discovered in 1887 by E. Rivière (Rivière, 1887) after railroad construction along the coast cut through the cliff, damaging and destroying a large part of the site. The remaining part of the site was excavated in stages over the last 40 years,

first in 1976 by Giuseppe Vicino (Vicino, 1984), second in 2002–2005 by Brigitte Holt and Fabio Negrino (Riel-Salvatore *et al.*, 2013; Holt *et al.*, 2019), and currently (2015 to present) by Julien Riel-Salvatore and Fabio Negrino (Riel-Salvatore and Negrino, 2018b). From bottom to top, the lower Mousterian stratigraphic units are labeled M1–M7, the upper Mousterian units MS1 and MS2, and the Protoaurignacian units A1–A3. These excavations revealed Late Mousterian deposits and bladelet-rich Protoaurignacian layers that appear undisturbed. The lithics found in the Mousterian layers share some similarities with the lithics found in the CSB, Gr and BM stratigraphic units at AV, suggesting potential contemporaneity between sites.

Micromorphological analyses show that instances of bioturbation appear to be more significant in the upper layers (MS1–M3) and are rare to non-existent in the lower layers (M4–M7; Fig. 2). Anthropogenic components such as charcoal, bone fragments or burned bone are absent at RB; however, flint is present in stratigraphic units M4–M6. Because flint does not naturally occur in the rock shelter and is probably indicative of stone tool production, this suggests there is more anthropogenic influence in these layers. Mineral constituents in each stratigraphic unit also contain variable amounts of aeolian and volcanic materials. Volcanic material is more common in the upper layers (MS1–M3) and some have been identified as highly altered porphyritic andesite. This material belongs to sediments outside of the rock shelter and also do not naturally occur within the shelter, suggesting input through aeolian processes.

Charcoal samples from exposed hearths were collected at RB and analyzed at Oxford University, the Max Planck Institute for Evolutionary Anthropology and Beta Analytic, Inc. (Higham *et al.*, 2014; Benazzi *et al.*, 2015; Holt *et al.*, 2019). Samples were calibrated using OxCal 4.2 (Bronk Ramsey, 2013) and the IntCal13 calibration dataset (Reimer *et al.*, 2013). Riel-Salvatore and Negrino (2018a) summarize all non-problematic dates present at RB. However, Holt *et al.* (2019) present samples (RB 47, 69, 265) that produced ages that were too young and do not agree with their cultural or geological context, which may be due to disturbances associated with the 19th century railroad construction. When considering non-problematic dates, the occupation of RB is dated to 44 000–36 000 cal a BP.

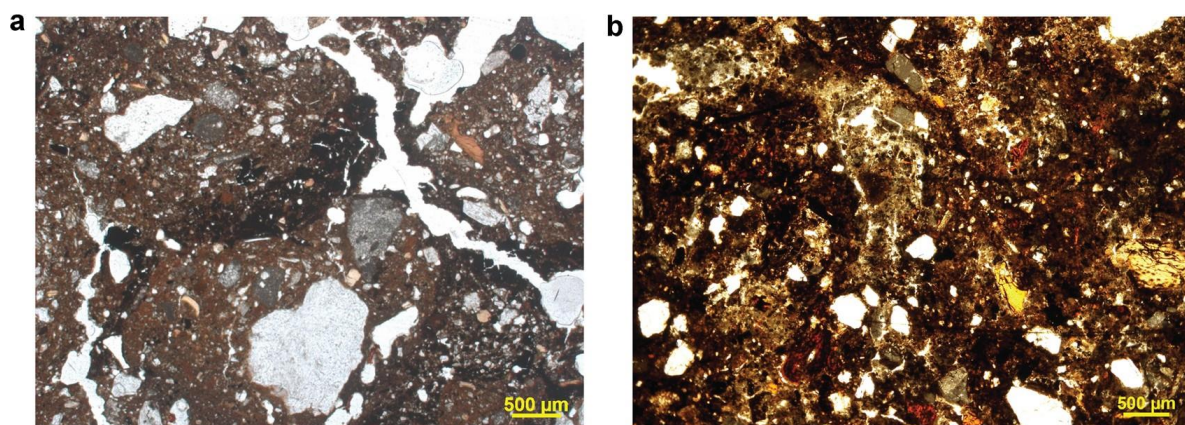


Figure 2. Photomicrographs from stratigraphic units in which cryptotephra shards were found at Arma Veirana and Riparo Bombrini. Both photos were taken in plane polarized light. (a) Photo of contact between BM and Gr stratigraphic units at AV. The dark organic lens (BM) shows mixing in the brown sediment (Gr), demonstrating that there is slight reworking between stratigraphic units. (b) Photo of stratigraphic unit M4 at Riparo Bombrini. Reworking is present as bioturbation forming the light-colored areas but is minimal.

Materials and methods

Cryptotephra sampling and extraction

In 2017 and 2018, we sampled for cryptotephra along exposed stratigraphic sections at AV and RB, following the methods of Lane *et al.* (2014). At both sites, we cleaned the sections and collected 10–20 g sediment samples from the bottom up in 2 cm intervals, creating continuously sampled columns. Each stratigraphic unit was sampled, resulting in approximately 1.5m of sample columns at AV (Supporting Information Fig. S1) and 1m at RB.

Samples were processed at the Cryptotephra Laboratory for Archaeological and Geological Research (CLAGR) at the University of Nevada Las Vegas (UNLV) using techniques published in Blockley *et al.* (2005). Major element compositions of individual tephra grains were determined using a JEOL JSX8900 SuperProbe electron probe micro-analyzer, equipped with four wavelength dispersive spectrometers, at the Electron Microanalysis and Imaging Laboratory at UNLV, following methodologies in Smith *et al.* (2018). Trace element analyses were completed at Michigan State University using a Thermo Scientific ICAP Q Quadrupole Inductively Coupled Plasma Mass Spectrometer integrated with a Photon Machines Analyte G2 193 nm excimer laser ablation system. Detailed methods are given in Appendix S1.

Statistical analyses

Statistical analyses were completed on cryptotephra compositional data using OpenBUGS (Lunn *et al.*, 2009), a Bayesian simulation software that uses Markov chain Monte Carlo (MCMC) routines to sample from the joint posterior distribution, following modified statistical methods from Smith *et al.* (2018) and Harris *et al.* (2017). For populations (P1,3 and P2) major and trace chemical data were modeled separately for each respective population. For P1,3, published chemical data from seven sources (i.e. marine core samples E-11, T1535, and I-2, Aeolian Islands – Falcone, Aeolian Islands – Punta del Perciato, Kirka-Phrigian Caldera, Acigöl – Korudag, Acigöl – Guneydag, and Campanian Ignimbrite) were used as the ‘reference data’ for which to compare unknown samples from AV and RB. E-11, T1535 and I-2 were grouped due to low sample size and because it is argued that these samples are all from the same eruption (see ‘Lipari Island, Italy’ for a discussion). Falcone and Punta del Perciato were analyzed separately in the model; however, they are referred to as one event (FPdIP) throughout the rest of this study due to being chemically similar (see ‘Lipari Island, Italy’ for a discussion). For P2, published chemical data from three sources (i.e. Oraefajökull or Torfajökull, Icelandic Rift Zone, and the Thorsmörk Ignimbrite), were used as the ‘reference data’ for which to compare unknown samples from AV and RB. A total of nine major elements and 20 trace elements were included in the respective models. Before running the model, all major oxide data were normalized to ensure that the comparisons between reference data were consistent. The full probability model describes the dependences

among the data and parameters that produce posterior distributions (1).

$$P(\mu, \Sigma, p | C) \propto P(C|\mu, \Sigma) P(\mu)P(\Sigma) \quad (1)$$

For each model, we assume the continuous trait data (C) arise from a multivariate normal distribution. A mean vector μ and covariance matrix Σ describe the covariation among quantitative traits. The mean variable vector μ is assumed to vary by source (e.g. Campanian Ignimbrite, E-11, T1535, etc.). Thus, for observation $I = 1, 2, \dots, N$, $c = 1, 2, \dots, C$ ($C = 9$) quantitative traits, and $s = 1, 2, \dots, 7$ sites, $P(C|\mu, \Sigma)$ is given as :

$$\begin{pmatrix} C_{1,i} \\ C_{2,i} \\ \vdots \\ C_{N,i} \end{pmatrix} \sim \text{Normal} \left(\begin{pmatrix} \mu_{1,s} \\ \mu_{2,s} \\ \vdots \\ \mu_{N,s} \end{pmatrix}, \Sigma \right) \quad (2)$$

We chose relatively non-informative conjugate priors for all quantities. An uninformative normal, Normal (0,10 000), prior was specified for each component of μ and a relatively non-informative Wishart (R,k) prior (Gelman et al., 2013) was chosen for the precision matrix ($\Omega = \Sigma^{-1}$), with degrees of freedom and R matrix corresponding to the number of variables used in each model (i.e. for Major and Trace models, $K = 9$ degrees of freedom and 20 degrees of freedom, respectively).

Table 1. Geochemical results for glass shard populations at Arma Veirana and Riparo Bombrini.

	P1(17)	SDEV	P2 (2)	SDEV	P3 (3)	SDEV
SiO ₂	76.83	0.80	76.30	0.73	76.82	0.16
TiO ₂	0.07	0.07	0.33	0.07	0.01	0.02
Al ₂ O ₃	12.70	0.46	11.77	0.71	12.18	0.34
Cr ₂ O ₃	0.03	0.04	0.00	0.00	0.00	0.00
FeO	0.67	0.13	2.49	0.23	0.81	0.10
MnO	0.05	0.04	0.05	0.07	0.08	0.04
MgO	0.02	0.02	0.08	0.01	0.01	0.01
CaO	0.81	0.21	0.84	0.04	0.70	0.13
Na ₂ O	3.61	0.21	2.96	0.12	3.87	0.54
K ₂ O	4.89	0.20	5.02	0.43	4.85	0.49
P ₂ O ₅	0.05	0.19	0.04	0.05	0.00	0.00
F	0.18	0.15	0.05	0.08	0.46	0.38
Cl	0.06	0.03	0.06	0.04	0.16	0.06
SO ₃	0.02	0.03	0.01	0.02	0.05	0.04
Total	97.21		93.55		94.82	
Ga	18.69	1.77	41.73		17.99	3.77
Rb	249.76	33.92	256.96		305.39	42.77
Sr	8.24	2.53	62.44		6.15	5.91
Y	55.77	12.11	94.01		111.90	31.77
Zr	110.60	20.09	956.35		138.61	19.87
Nb	35.28	10.76	78.59		41.84	4.68
Cs	4.88	0.99	6.75		7.51	0.42
Ba	4.23	2.73	1730.95		4.14	5.04
La	16.61	3.17	128.26		9.56	2.26
Ce	37.85	3.70	300.20		27.69	4.52
Pr	5.31	0.91	32.28		3.53	1.05
Nd	20.21	2.14	118.22		18.34	3.53
Sm	5.77	1.28	28.85		7.96	1.42
Eu	0.23	0.21	3.09		0.06	0.11
Gd	5.75	2.12	21.34		9.54	1.90
Tb	1.17	0.17	4.36		1.85	0.38
Dy	7.49	1.74	21.33		14.19	3.09
Ho	1.55	0.45	4.51		3.44	1.04
Er	5.15	1.38	14.90		11.75	2.98
Tm	0.91	0.29	1.90		3.73	4.79
Yb	6.16	2.21	14.08		20.50	18.34
Lu	1.08	0.39	1.96		1.90	0.44
Hf	4.86	0.81	25.43		7.79	1.99
Ta	3.61	1.77	7.14		3.94	0.37
Pb	35.77	2.90	29.53		39.67	3.38
Th	27.30	4.38	29.39		34.43	4.18
U	6.42	1.12	6.53		8.45	0.85

Compositions present are averages. All data are presented in Table S1. SDEV =one standard deviation.

P1 =population 1, P2 =population 2, P3 = population 3.

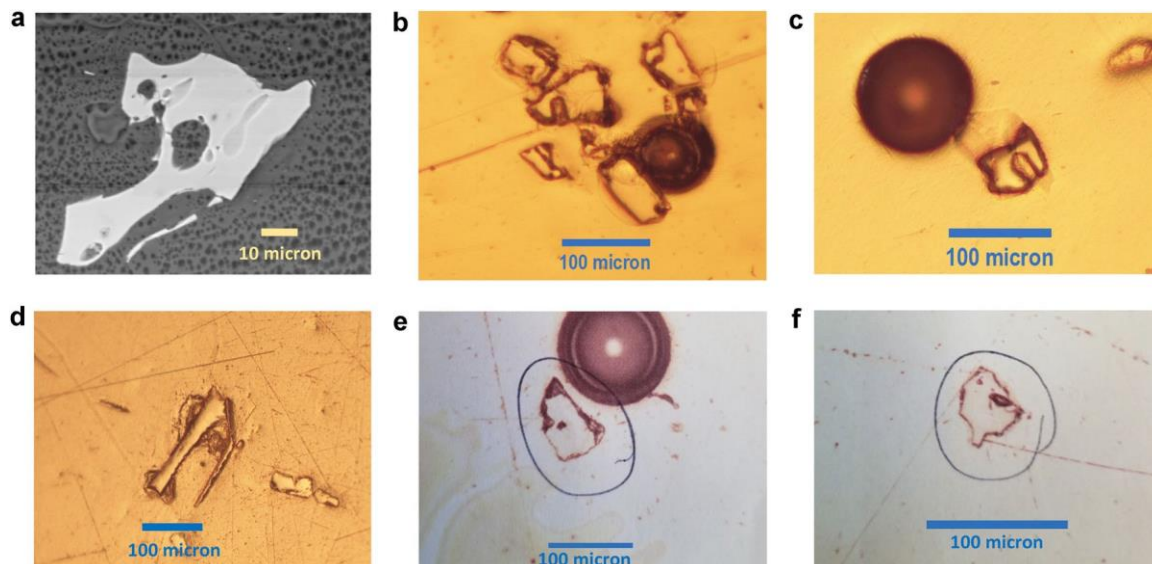


Figure 3. Examples of cryptotephra from Arma Veirana and Riparo Bombrini. Images were taken from polished epoxy rounds using plane-polarized light. Image (a) was taken using scanning electron microscopy with back-scattered electrons. (a) Shard from sample AV662 (P1). This is a high-resolution backscattered electron image. (b) Shards from sample AV651 (P1). (c) Shard from sample AV655 (P1). (d) Shard from sample AV665 (P2). (e,f) Shards from sample RB15a (P3).

We tested our two models' predictive ability by randomly dividing each reference dataset, of known volcanic eruptions, into two subsets, 'training' data and (90%) and 'validation' data (10%), to perform multiple out-of-sample cross validations. The process was repeated five times for each model to produce an average out-of-sample cross validation for each model. Following model validation, the two data subsets were combined and used to examine the archaeological samples. For the major element data, 17 samples were from AV and three samples were from RB. For the trace element data, five samples were from AV and six samples were from RB.

To determine whether P1 from AV and P3 from RB are derived from the same or different populations, we performed a multivariate analysis of variance. Since these data violate the assumption of multivariate normality and the number of variables exceeds the number of samples, we carried out a non-parametric analysis of variance (NP-MANOVA) using the software package *npnv* (Ellis *et al.*, 2017) within the R programming environment (v.3.3.3; R Development Core Team, 2017).

Results

AV and RB cryptotephra horizons

There are two cryptotephra populations present at AV (P1 and P2) and one cryptotephra population at RB (P3) (Figs. 4,5). At both sites, the shards are high-silica rhyolites (Tables 1 and S1) and are in extremely low abundance (1–8 shards g^{-1}). P1 is characterized by 75.09–78.32 wt.% SiO_2 , 11.6–13.47 wt.% Al_2O_3 , 0.44–0.91 wt.% FeO and a $K_2O/Na_2O > 1$ and P2 by 75.78–76.82 wt.% SiO_2 , 11.27–12.27 wt.% Al_2O_3 and 2.33–2.65 wt.% FeO. P3 has concentrations of 76.64–76.96 wt.% SiO_2 , 11.79–12.44 wt.% Al_2O_3 , 0.7–0.89 wt.% FeO and a $K_2O/Na_2O > 1$. Trace element analyses for P1 and P3 show depletions in Ba and Sr, an Eu anomaly and enrichment in heavy rare earth elements (HREE) (Fig. 6b). For P2, trace element analyses show a depletion in Sr and an enrichment in light rare earth elements (LREE) (Fig. 10). At AV, P1 was found in stratigraphic units BM and Gr and is the most common shard composition. Shards are small ($<100 \mu m$) and appear to be rounded when viewed in epoxy mounts, but several show angular and cusped margins. The shards are entirely glass, lack phenocrysts and several contain small vesicles (Fig. 3). A shard count profile of P1 displays a few distinct peaks concentrated in the BM (Fig. 4). Sample AV651 shows the highest peak and was collected at the base of the exposed stratigraphic section. P2 is in stratigraphic unit Gr in sample AV665. These shards are larger than P1 ($>100 \mu m$) and are tabular with sharp angular corners (Fig. 3). There were not enough P2 shards to generate a count profile (fewer than three shards).

At RB, P3 was found in stratigraphic units M1–M4 in extremely low abundance (3 shards g^{-1}) (Fig. 5). Shards are small ($\sim 80 \mu m$) and well-rounded (Fig. 3) and are most abundant in units M4/M3 (Fig. 5).

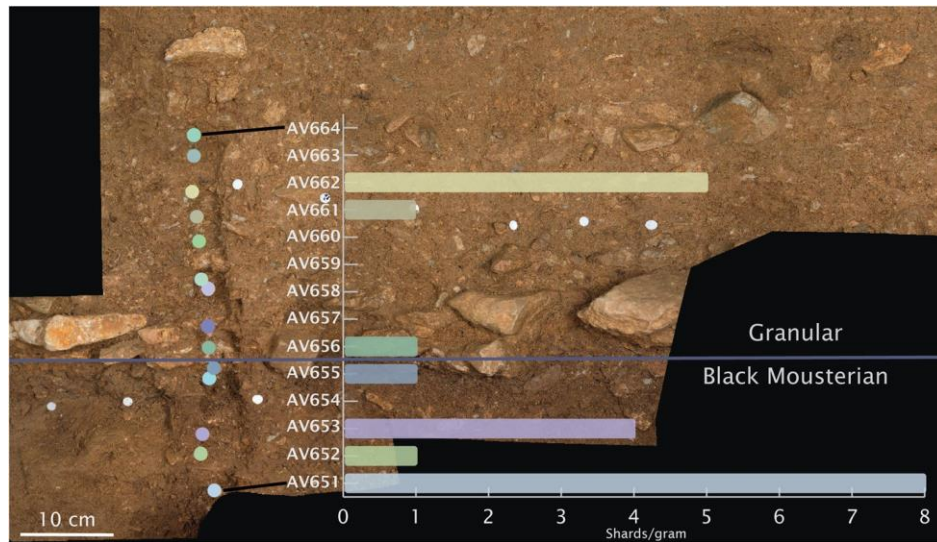


Figure 4. Shard concentrations at Arma Veirana. Samples AV651 to AV662 contain P1 shards. The y-axis represents each sample number and the x-axis shows shards per gram.

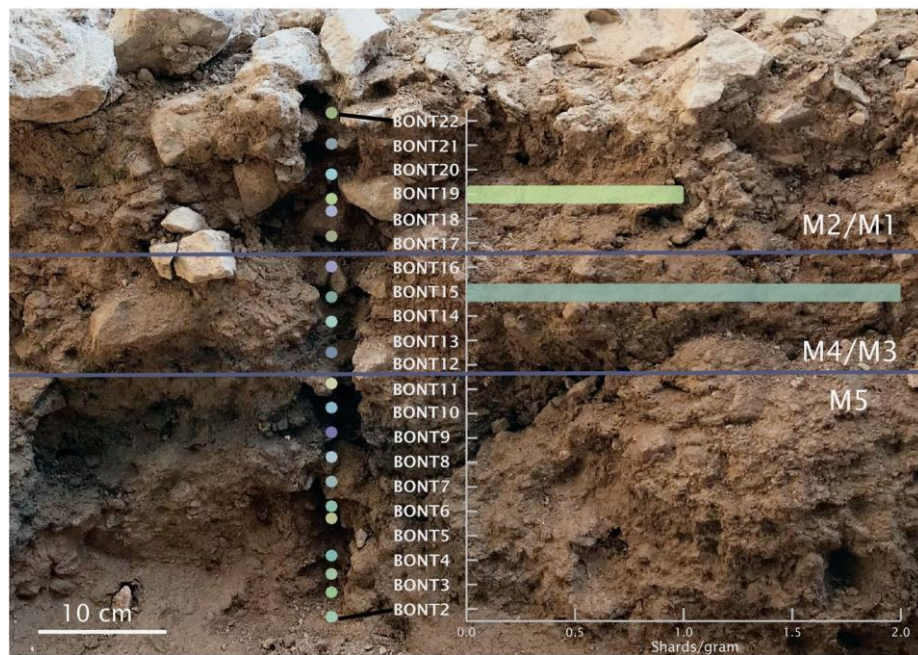


Figure 5. Shard concentrations at Riparo Bombrini. Samples BONT15 to BONT19 are attributed to p3 and are present in stratigraphic units M1–M4. The y-axis represents each sample number and the x-axis shows shards per gram.

Comparison of AV and RB shard chemistry

P1 and P3 shards are high-silica, calc-alkaline rhyolite with $\text{FeO} < 1$ wt.%, $\text{K}_2\text{O}/\text{Na}_2\text{O} > 1$ and $\text{Zr}/\text{Nb} < 5$ (Fig. 6) and are atypical of rhyolite erupted from volcanoes in the Mediterranean region. The shards lack a distinctive Nb–Ta trough characteristic of subduction zone magmatism and are more typical of intraplate volcanism. P2 shards are also high-silica, calc-alkaline rhyolites but with 2.33–2.65 wt.% FeO and $\text{Zr}/\text{Nb} > 5$ (Fig. 6). The trace element signature of P1 and P3 is nearly identical and it is very distinctive with depleted LREE, a deep Eu anomaly, enriched HREE, and strong depletion in Ba and Sr. The nearly identical major and trace element signatures of P1 shards (AV) and P3 shards (RB) indicate that they are probably related to the same eruptive event. Using NP- MANOVA, we found there are not significant differences in the compositions of major element chemistry between the two populations, suggesting that P1 and P3 belong to the same population ($F = 2.20$, $\text{df}_1 = 1.40$, $\text{df}_2 = 9.95$, $p = 0.167$, $\alpha = 0.05$). Therefore, we group them for the purpose of locating a source and will refer to them as P1,3. P2 shows a very distinct geochemical signature that is probably derived from an eruption in a different region.

The P1,3 trace element signature (especially depleted LREE and enriched HREE) is rare and is mainly found in intraplate rhyolites with high fluorine content that have undergone extensive crystal fractionation (Christiansen *et al.*, 2007; Jowitt *et al.*, 2017) or created by fractionation of rare-earth-bearing minerals such as allanite (Miller and Mittlefehldt, 1982). Many of these rhyolites are associated with economic mineral deposits (reviewed by Jowitt *et al.*, 2017). The Ba, Sr and Eu troughs are due to fractionation of feldspar. The trace element signature for P2 shows enriched LREE (Fig. 10) and follows similar trends to volcanoes on the western and eastern side of Iceland, which are located on the flanks of a rift (Jakobsson *et al.*, 2008).

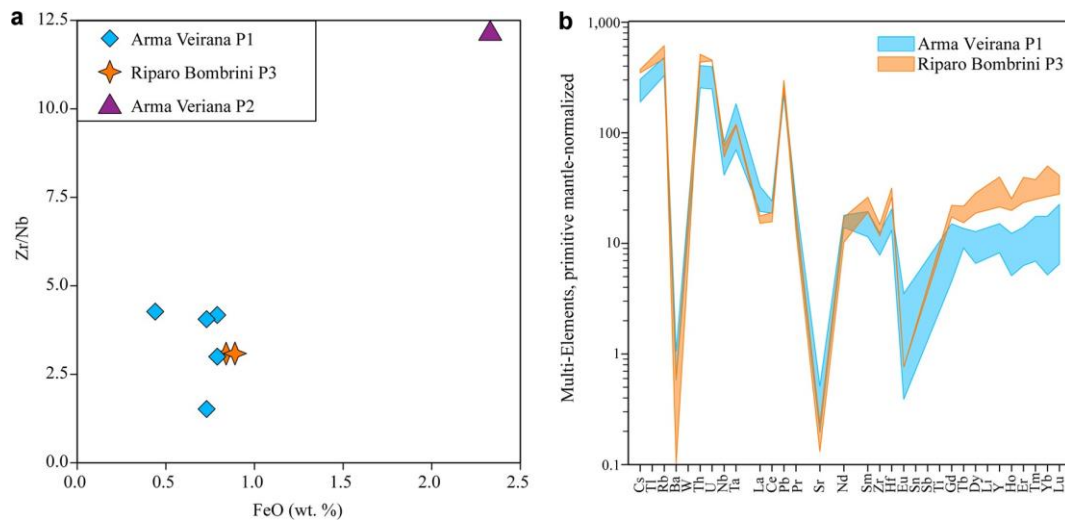


Figure 6. Geochemical comparisons of P1 (Arma Veirana) and P3 (Riparo Bombrini). (a) Comparison of major element chemistry of P1 and P3 shards. FeO (wt%) vs. Zr/Nb (p.p.m.). (b) Comparison of trace element chemistry of P1 and P3. Trace element data are normalized to primitive mantles of Sun and McDonough (1989).

Source of the shards

Locating potential sources

Based on the geochemistry of the shards and lack of similar proximal sources, locating a source volcanic eruption for P1,3 (AV and RB) and P2 shards required a worldwide search for eruptions with a comparable major and trace element chemistry (Tables S2 and S3). We searched the databases of the ‘Volcano Global Risk Identification and Analysis Project’ (VOGRIPA; <https://www.bgs.ac.uk/vogripa/index.cfm>), ‘RE- Sponse of humans to abrupt Environmental Transitions’ (RESET; <http://c14.arch.ox.ac.uk/reset>), ‘Integrating ice cores, marine and terrestrial records’ (INTIMATE; <https://c14.arch.ox.ac.uk/intimate/db.php>) and the Smithsonian Institute’s ‘Global Volcanism Program’ (<https://volcano.si.edu/>) for volcanic compositions similar to P1,3 and P2 shards. We also performed an extensive literature search (Table S2) which resulted in the generation of a reference dataset specific to sourcing P1,3 and P2 (Table S3). We included the Campanian Ignimbrite and Massif Central when compiling data, although this was mainly for exclusionary purposes due to the widespread exposure in the region.

Ideally, major and trace element chemistry should be sufficient to match cryptotephra to a source, but for P1,3, several volcanic areas are candidate sources and because most analyses for the comparison volcanoes are whole rock and not glass, we considered other factors such as age of the enclosing sediments, shape and freshness of shards, and ease of transport from the source volcano to the site of deposition in our search for a source. We searched for eruptions in a variety of tectonic settings; however, volcanic fields located in an intraplate or back-arc setting were favored due to the lack of a negative Nb–Ta anomaly, characteristic of subduction-related volcanism (White, 2013). Due to the poor age constraint at AV and RB, we included a wide range of ages in our search (Tables S2 and S3). Important parameters for a chemical match of P1,3 shards to a possible source are $\text{SiO}_2 > 75$ wt.%, $\text{FeO} < 1$ wt.%, $\text{K}_2\text{O}/\text{Na}_2\text{O} > 1$, primitive mantle-normalized Nb/Ta < 1 , depletion in Ba, Sr, Eu and LREE, and enrichment in U and Th compared to primitive mantle. Parameters for a chemical match of P2 shards are $\text{SiO}_2 > 75$ wt.%, $\text{FeO} > 2$ wt.%, $\text{K}_2\text{O}/\text{Na}_2\text{O} > 1$, depletion in Sr and Eu and an enrichment in LREE relative to primitive mantle. We narrowed the list of possible sources for P1,3 shards to three volcanic fields and two volcanoes for P2 based on similarities in composition and tectonic setting. Possible sources for P1,3 are the Acigöl volcanic field in Turkey, the Kirka-Phrigian Caldera in central Turkey and eruptions on Lipari Island, Italy. For P2, possible sources are Öraefajökull or Torfajökull in Iceland. We built a Bayesian statistical model to assign a probability that individual shards from P1,3 and P2 belong to one of the possible sources.

Statistically distinguishing sources

After removing the burn-in period (‘burn-in’ refers to the initial number of MCMC iterations before chain convergence), our Bayesian model predicted the source of each ‘unknown’ sample (i.e. P1,3 and P2 shards). Accurate assignment of sources was determined according to the highest probability of assignment. The results of the out-of-sample cross validation for each of the models is given in Table 2.

Upon assessing model performance, training and validation subsets were recombined and used to predict archaeological samples. For P1,3, Model 1a (P1,3 Major) assigned 18 of the samples as being derived from the E-11, T1535 and I-2 samples and two of the samples as being derived from the Acigöl-Guneydag (Table S4). Model 1b (P1,3 Trace) assigned four of the P1,3 samples as belonging to the Punta del Perciato volcanoes, two samples to Kirka-Phrigian Caldera, two samples to Acigöl-Guneydag and one sample to Acigöl-Korudag (Table S4).

For P2, Model 2a (P2 Major) predicted the two archaeological samples as belonging to the Icelandic Rift Zone (Table S4). Model 2b (P2 Trace) assigned the archaeological sample as belonging to each of the populations equally, as indicated by the equal probability of assignment for all three eruptions (Table S4).

Acigöl Complex, Anatolia

The Acigöl Complex, located in central Anatolia, is similar in major and trace compositions to P1,3 (Figs 7,8). Various eruptions and deposits of the Acigöl Complex were examined as potential sources (i.e. Young Dome, Korudag, Bogazköy, lower Acigöl Tuff, upper Acigöl Tuff, Kaleci, Tepeköy, Guneydag, Kuzay and Karniyarik) that range in age from 200 to 20 ka (Druitt *et al.*, 1995; Tryon *et al.*, 2009, 2011; Siebel *et al.*, 2011). Compositions of some of the younger eruptions (i.e. Karniyarik, Kuzay, Korudag) are closer in major and trace composition to P1,3 than the older eruptions (i.e. lower Acigöl Tuff, upper Acigöl Tuff, Bogazköy). Therefore, we

included Guneydag and Korudag in our Bayesian model because we were able to obtain major and trace chemical data and they were compositionally most similar to AV and RB (Druitt *et al.*, 1995; Siebel *et al.*, 2011). The model assigned relatively low probabilities to Guneydag and Korudag, suggesting a low likelihood that the archaeological samples derive from these eruptions (Table S4). While both major and trace element concentrations for the younger (20 ka) eruptions in the Acigöl Complex appear to match P1,3 chemistry, there are several factors that rule out this area as source. First, the eruptions occurred during tuff-ring formation before the extrusion of rhyolite domes. These eruptions were low in volume and unlikely to spread tephra far from the source (A. Schmitt, 2019, unpublished data). Second, tephra transport from Turkey to Italy is east to west against prevailing atmospheric circulation. We suggest that transport of low-volume tephra in this direction is unlikely. Third, trace element chemistry was analyzed by X-ray fluorescence spectrometry and not laser-ablation inductively coupled plasma mass spectrometry. Lastly, our Bayesian model does not assign high probabilities to any Acigöl eruptions (Table S4). Although these data may be reliable, it is not appropriate to compare datasets obtained by different analytical methods. Therefore, we rule out eruptions from the Acigöl Complex as the source of P1,3 shards.

Table 2. Average performance for five out-of-sample cross validation runs for each of the four models applied to P1,3 and P2. DEV = one standard deviation.

	Population	Average model performance (SDEV)
Model 1a	P1,3 major	0.80 (0.088)
Model 1b	P1,3 trace	0.833 (0.163)
Model 2a	P2 major	0.975 (0.056)
Model 2b	P2 trace	1 (0)

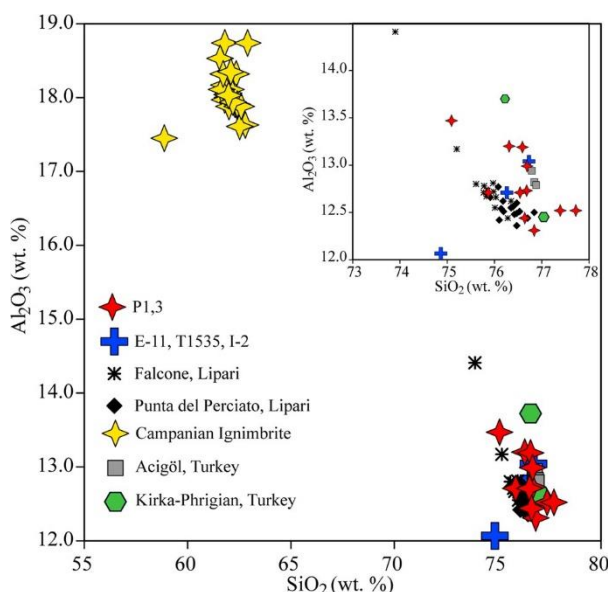


Figure 7. Geochemical comparisons of P1,3 and potential sources. SiO₂ vs Al₂O₃ (wt%). Plot in top right corner excludes the Campanian Ignimbrite.

Kirka-Phrigian, Anatolia

We also considered the possibility that P1,3 shards were reworked from local sedimentary rocks that contain tephra from Miocene eruptions. One possible source of Miocene shards is ash-flow tuff erupted during formation of the Kirka-Phrigian Caldera in western Anatolia at about 18 Ma (Seghedi and Helvacı, 2016). Both major and trace element whole rock data provide a potential match to P1,3 (Figs 7,8) and it is possible that a caldera-forming event of this magnitude could have spread tephra across Europe. However, this match is based on a comparison of glass to whole rock data, and glass analyses for the Kirka-Phrigian tuffs are required to make a more robust correlation. Additionally, our Bayesian model assigned only three samples to the Kirka-Phrigian Caldera, suggesting a small likelihood of assignment (Table S4). Therefore, there are various factors that rule out Kirka-Phrigian as a source for P1,3. Transport of tephra from Kirka-Phrigian to Italy involves a complex series of events. The incorporation of Kirka-Phrigian shards in AV–RB sediment requires that the caldera eruption spread tephra across Europe in the Miocene. Then, the tephra would have to be stored in Miocene sediments like those described in western Italy in the Po Valley (Ruffini *et al.*, 1995). Lastly, shards would have to be eroded from these deposits, transported and deposited at AV and RB simultaneously. We consider this sequence of events to be very unlikely. Shards are delicate and easily altered and thus would probably lose their delicate angular sharp edges and vitric interiors if subjected to long-distance transport by alluvial, aeolian and soil formation processes.

Lipari Island, Italy

While Italy is an obvious source candidate, magmatic provinces, except those in the Aeolian Islands, are mainly subduction related and tend to be alkaline to ultrapotassic and have higher FeO and LREE concentrations than P1,3 shards (Peccherillo, 2005). Other areas in the Mediterranean (i.e. Aegean Sea, Marmara Sea, Greece) are also dominated by subduction zones and show significant differences in trace elements when compared to P1,3 and P2 (Aksu *et al.*, 2008; Tomlinson *et al.*, 2012; Satow *et al.*, 2015; Koutrouli *et al.*, 2018). However, the tectonic setting of Lipari Island in the Aeolian Island chain is somewhat controversial. Chiarabba *et al.* (2008) suggest that Aeolian Island volcanism is related to post-subduction back-arc extension with an inactive subducted slab at depth, making it a potential source for P1,3 shards.

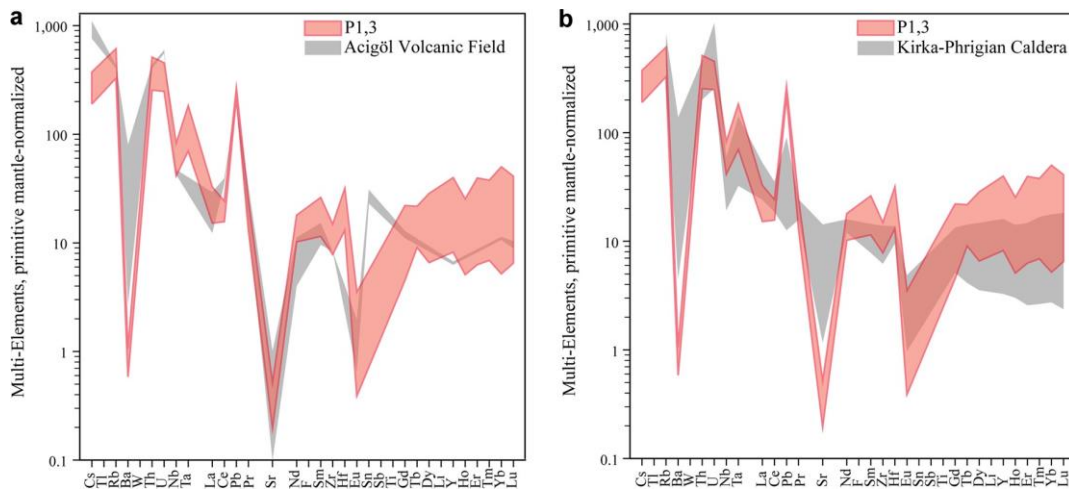


Figure 8. Comparison of trace element chemistry of P1,3 and other potential sources. (a) Comparison of trace element chemistry of P1,3 shards to rhyolite from the Acigöl volcanic field. Trace element data are normalized to primitive mantles of Sun and McDonough (1989). (b) Comparison of trace element chemistry of P1,3 shards to rhyolite from the Kirka-Phrigian caldera. Trace element data are normalized to primitive mantles of Sun and McDonough (1989).

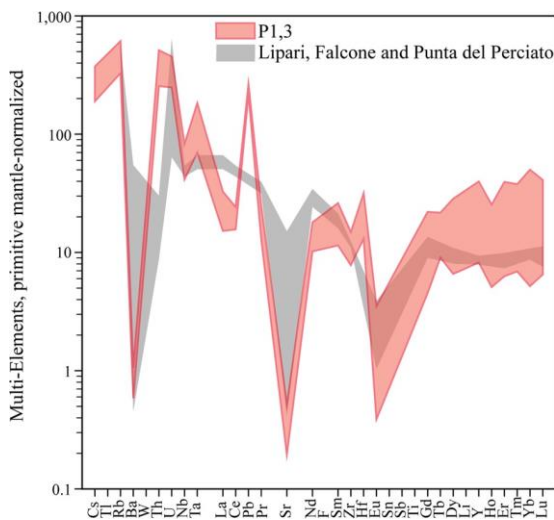


Figure 9. Comparison of trace element chemistry of P1,3 shards to Lipari Island volcanoes. Data for Falcone volcano and Punta del Perciato are retrieved from Albert *et al.* (2017). Trace element data are normalized to primitive mantles of Sun and McDonough (1989).

The Lipari Volcanic complex in the Aeolian Islands formed between 267 ka and AD 776–1220 (Forni *et al.*, 2013). Volcanoes erupted calc-alkaline basaltic andesite to rhyolite with rhyolite being dominant for the last 43 ka. Eruptions from two of these volcanoes, Falcone (43–40 ka) and Punta del Perciato (56–43 ka), produced chemically identical high-silica rhyolite domes and pyroclastic deposits (FPdelp). We compared trace elements of the P1,3 to tephra produced by FPdelp compiled by Albert *et al.* (2017). Using a multi-element plot normalized to primitive mantle (Fig. 9) both P1,3 and FPdelp tephra show depletion in Ba, Sr and Eu, suggesting magmatic fractionation of feldspar (probably K-feldspar). Both have Nb/Ta < 1 and enriched U contents. P1,3, however, is depleted in LREE and slightly enriched in HREE compared to FPdelp. Also, Th is lower in P1,3 than FPdelp. REE differences at first appear to invalidate a correlation but may be explained if P1,3 represents a highly fractionated explosive phase of the FPdelp eruption. A common way of producing LREE depletion in rhyolite is mineral fractionation of REE-rich accessory minerals such as allanite and monazite and to a lesser extent apatite and zircon (Miller and Mittlefehldt, 1982). Both allanite and monazite become saturated in rhyolitic magma at low concentrations, and because of their small size and low abundance, they are easily overlooked in thin sections using traditional optical methods. Allanite and monazite fractionation occur in the upper, more highly fractionated and volatile-rich part of a magma chamber that is erupted explosively early in an eruption (Miller and Mittlefehldt, 1982). Shards produced by such an eruption would be carried in the eruptive plume and eventually distally deposited. This event may not be recorded in proximal deposits. We suggest that the LREE depletion in P1,3 formed in this manner and that P1,3 represents a highly fractionated early erupted component of the eruption related to FPdelp.

An example of a tephra unit erupted from Lipari but not recorded in the stratigraphic record on the island is unit E-11, discovered in the Tyrrhenian Sea Marine Core KET8003 (Paterne *et al.*, 1988). The tephra is dated to 37.7 ka, it occurs directly above the 39 ka Campanian Ignimbrite (CI) (De Vivo *et al.*, 2001), and it may be a widespread marker bed. Albert *et al.* (2017) correlated E-11 to chemically similar tephra in marine cores from the Ionian Sea as unit T1535 (Matthews *et al.*, 2015) and I-2 (Insinga *et al.*, 2014). Although only major element chemistry is available for tephra from these marine core units, they are probably associated with the FPdelp volcanoes on Lipari Island (Albert *et al.*, 2017). Major elements for E-11, T1535 and I-2 are similar to P1,3 (Fig. 7; Table 3). All are high-silica, low-FeO rhyolites with K₂O/Na₂O > 1. CaO concentrations are lower than P1,3 but fall within one standard deviation of mean P1,3 values. Overall this marine core tephra compares well with P1,3. Albert *et al.* (2017) ruled out a direct correlation with proximal units because FPdelp rhyolites are more elevated in K₂O than E-11, older than E-11 and pre-date the CI, whereas E-11 overlies the CI. Albert *et al.* (2017) suggest that E-11 may represent a younger eruption from Falcone, but all evidence of this eruption on Lipari was erased by even younger eruptions from Monte Guardia. Therefore, the tephra record in the marine core may provide a better historical eruption record than found proximally on Lipari.

Eruptions from Lipari Island are the most likely source for P1,3 for the following reasons. First, the age of eruptions (56–37.7 ka) is

compatible with the age assumed for sediments at RB and AV. Second, northward transport of tephra from Lipari to north-west Italy is well documented. In fact, E-11 is found in the Tyrrhenian Sea in a marine core to the north of Lipari Island. Third, the chemical match between FPdelP and E-11 and P1,3 is not perfect, but major elements are very similar and, as discussed, P1,3 may represent an early explosive phase related to the FPdelP event. Our Bayesian Model 1a (major chemical data) assigned a high probability of samples being derived from E-11, T1535 and I-2, whereas Model 1b (trace chemical data) assigned a high probability of samples being derived from Punta del Perciato. Unfortunately, the record of eruptive events on Lipari Island is incomplete due to erosion or non-deposition, so there is no record of this explosive phase on Lipari Island. Despite the incomplete record, the 56–37.7 ka Lipari eruptions still represent the best match to P1,3 based on age, compatibility with the age of AV and RB sediments, ease of transport and chemistry. Determining the specific Lipari eruption responsible for P1,3 is desirable. Future work will focus on obtaining trace elements on glass shards associated with FPdelP dome eruptions and marine core samples.

Table 3. Major element chemistry of possible sources and comparison to P1,3.

	E-11*	T1535 [†]	I-2 [‡]	Mean P1	Mean P3	Falcone [§]	Punta del Perciato [§]
SiO ₂	76.73	76.92	76.26	76.83	76.82	76.28	76.47
TiO ₂	0.06	0.09	0.06	0.07	0.01	0.06	0.04
Al ₂ O ₃	13.04	12.40	12.71	12.70	12.18	12.44	12.36
FeO [¶]	1.01	1.31	1.34	0.67	0.81	1.50	1.16
MgO	0.06	0.03	0.03	0.02	0.01	0.01	0.01
CaO	0.65	0.65	0.71	0.81	0.70	0.72	0.69
Na ₂ O	3.27	3.73	3.48	3.61	3.87	3.33	3.37
K ₂ O	5.05	4.84	4.95	4.89	4.85	5.60	5.77
Total	99.87	97.32	95.51			95.34	95.64

*E-11 (Paterne *et al.*, 1988).

[†]T1535 (Matthews *et al.*, 2015).

[‡]I-2 (Insinga *et al.*, 2014).

[§]Falcone and Punta del Perciato (Albert *et al.*, 2017).

[¶]For E-11, reported as Fe₂O₃ converted to FeO

‘Total’ is the pre-normalized analytical total.

Öraefajökull and Torfajökull, Iceland

The same potential sources were examined for P2 as for P1,3. Some sources were easily eliminated due to the higher FeO values (> 2 wt.%) and different trace element values than P2. For P2, the most probable source eruptions are from Iceland (Fig. 10). Multiple tephra deposits from a marine core collected in the North Atlantic show geochemical similarities to P2 (Abbott *et al.*, 2014). Deposits range in age from Marine Isotope Stage (MIS) 6 to MIS 4 (190–70 ka) and have been linked with nearby cores (i.e. ENAM33). Potential source volcanoes are Öraefajökull or Torfajökull; however, exact eruptions are not yet determined. Compositions from various deposits throughout Iceland were also considered (Jónasson, 2007; Martin and Sigmarsson, 2007). Data from these analyses show similarities in trace elements for Torfajökull and P2, further confirming this area as a source (Fig. 10). The primitive-mantle plot (Fig. 10) shows that both Torfajökull and P2 are slightly depleted in Cs, Rb, Ba, Th and U. Therefore, the shards from P2 could have originated from Torfajökull, although these results are tentative. Our Bayesian model results for Models 2a and 2b were inconsistent with the above results. Additionally, Model 2b assigned the archaeological samples as belonging to each potential source equally. An equal assignment is essentially inconclusive and indicates that more work needs to be done. Increasing the size of the model comparison database may help to statistically distinguish between sources for P2.

Discussion

Problems with interlaboratory data comparisons

Compiling compositional data from published sources can be difficult due to the differences in how laboratories analyze and report chemistry. While the development of large-scale databases (e.g. the RESET Project, VOGripA, INTIMATE) and interlaboratory studies (Kuehn *et al.*, 2011) are critical steps forward, differences in the type of materials analyzed make it difficult to directly compare data from various sources. Table S2 lists the various techniques used and materials analyzed, further demonstrating the variability from one laboratory to the next. While analytical conditions are often reported, variations in analytical techniques must be considered when comparing data. Additionally, caution is needed when comparing whole-rock data to glass data, as results depend on the crystal content in the whole-rock samples. If the percentage is small, then the whole-rock data should be very similar to glass data (White, 2013). However, glass can contain compositional heterogeneity that is sometimes not preserved in whole-rock samples and, when compared, glass chemistry will be depleted in compatible elements and enriched in incompatible elements (Tomlinson *et al.*, 2015). To account for this issue, examining trace ratios such as Zr/Nb and Ba/Nb can be helpful. If the phenocrysts are in equilibrium with the liquid, these ratios should stay consistent in both liquid and crystals, providing a temporary solution until more data are available. Therefore, the sources suggested in this study are based on data obtained by different laboratories at different times and eventually need verification by analyzing all samples in the same laboratory using the same analytical techniques and parameters.

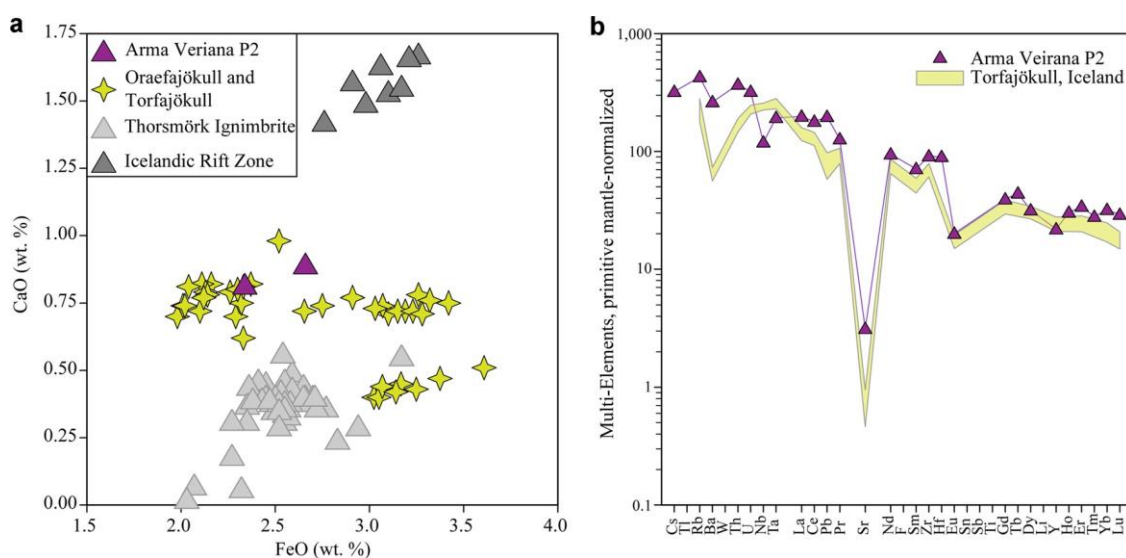


Figure 10. Geochemical comparison of P2 and potential sources. (a) FeO vs. CaO (wt.%). Data were retrieved from Abbott *et al.* (2014), Martin and Sigmarsson (2007) and Tomlinson *et al.* (2010). (b) Trace element chemistry of P2 shards to rhyolite from Torfajökull (data from Abbott *et al.*, 2014). Trace element data are normalized to primitive mantles of Sun and McDonough (1989).

Distinguishing primary and reworked tephra

Shard count profiles are the main method to determine whether tephra was deposited by primary processes and if there is reworking. When dealing with extremely low abundance shards, micromorphological analyses are also useful to better understand the amount of reworking between stratigraphic units as well as how the deposits accumulated at each site (Smith *et al.*, 2018). This type of analysis aids in quantifying what depositional and post-depositional processes may have affected the shards.

A shard count profile was developed only for P1 and P3 (Figs 4,5) due to low abundance (<3 shards g^{-1}) for P2. The shard count profile for P1 at AV displays few distinct peaks in the BM and Gr, with the vast majority of shards in the BM. Because the highest shard count is at the base of the section, it is possible that more shards continue below the collected section, which has not yet been excavated. The contact between the BM and Gr appears sharp in the field, but under the microscope the contact is a transitional zone 1–2 cm wide. The nature of this contact demonstrates that there is no significant mixing between BM and Gr. The shard count profile for P3 at RB displays one peak in stratigraphic units M4/M3 (Fig. 5). Micromorphological analyses at RB show minimal bioturbation of the sediments, suggesting shards have not been significantly reworked since deposition.

An exact isochron location is still under investigation due to extremely low abundance shard counts and the hypothesis that P1 shards continue below the collected section, and it will be confirmed through further excavations. Regardless, there are chemically similar shards at AV and RB which have not experienced serious reworking, and most shards are present in culturally similar stratigraphic units (i.e. BM and M4/M3). These results provide a way to temporally link both sites and if this chemically distinct cryptotephra represents a widespread distal unit, it could provide an important marker horizon for linking other Middle–Upper Paleolithic sites throughout the region.

Archaeological implications for discovering shards at AV and RB

The Middle–Upper Paleolithic transition is a difficult period to date. Currently, most sites that preserve these records have been dated using radiocarbon techniques (Higham *et al.*, 2014); however, the dating limit of radiocarbon (50–40 ka) falls at the middle of that transition (Higham *et al.*, 2009; Higham, 2011). Moreover, radiocarbon dates are commonly susceptible to contamination and can result in underestimations of the correct age (Higham, 2011). Despite methodological advancements (Higham *et al.*, 2014), the issues surrounding radiocarbon dating near its limit require archaeologists to use complementary dating and correlation methods. Therefore, the discovery of the same cryptotephra (P1,3) at AV and RB can be used to test calculated dates (i.e. radiocarbon) as well as provide a potential marker horizon between deposits at archaeological sites that date to the Middle–Upper Paleolithic. Other archaeological sites such

as Riparo Mochi, Arma delle Mànie, and Grotta degli Zerbi that are potentially coeval with AV and RB would be good candidates for future cryptotephra analyses. These sites are within 100 km of AV and RB and, based on current dates, overlap in occupational periods (Kuhn and Stiner, 1998; Cauche *et al.*, 2002; Cauche, 2007; Douka *et al.*, 2012; Negrino *et al.*, 2018). It will also be useful to search for P1,3 shards in various lacustrine core archives (e.g. Lago de Grande di Monticchio, Lake Orchid) to better understand the geographical extent of this tephra horizon (Wulf *et al.*, 2004; Wagner *et al.*, 2008). By locating P1,3 in various other deposits, archaeologists can begin to study the Middle–Upper Paleolithic transition at a larger scale instead of conducting site-specific studies.

Conclusions

The use of cryptotephra in archaeological studies is advancing how scientists date and correlate archaeological sites over large distances. Tephra studies have become especially important as many sites rely on radiocarbon dating even when deposits are close to the method's limit (50–40 ka). In this contribution, we used tephrochronology to correlate the occupational histories at two Middle–Upper Paleolithic sites, AV and RB. These sites are located 80 km apart and contain similar cultural industries, suggesting contemporaneity. We sampled both sites with the goal of finding shards of the same composition, allowing a direct comparison of deposits. We also integrated micromorphological studies to our analysis to better understand the depositional and post-depositional processes that may have affected the location of shards.

Our work resulted in the discovery of two shard populations (P1 and P2) at AV and one population (P3) at RB. Geochemical analyses showed that P1 is from the same eruption as P3, providing a unique marker between deposits. We suggest that P1,3 shards represent a highly fractionated early erupted component of 56–37.7 ka rhyolite from Lipari Island. P2 shards show a depletion in Sr and an enrichment in LREE which is probably derived from Torfajökull in Iceland; however, we have not identified the exact eruption. The most important result is the identification of P1,3 at both AV and RB, allowing a tool to test the amount of overlap between deposits. As discussed above, the exact isochron location is not yet determined due to extremely low abundance (<4 shards g⁻¹) of shards in P3 and uncertainty regarding the distribution of shards in P1. Micromorphological results show minimal reworking at both sites, suggesting the location of shards are reliable. Despite these results, more shards need to be identified to refine the isochron and future excavations will focus on this.

This study highlights how cryptotephra can be used to link archaeological deposits and test the validity of other dating methods even without identifying a specific source eruption. The chemistry of P1,3 shards is distinctive and unusual for European volcanoes. This particular marker will be important for answering questions pertaining to the Middle–Upper Paleolithic transition and correlating other Paleolithic sites throughout Europe.

Supporting information

Additional supporting information may be found in the online version of this article at the publisher's web-site.

Table S1. Geochemical data of P1, P2, and P3.

Table S2. List of reference tephra.

Table S3. Compiled data used for sourcing tephra.

Table S4. Bayesian model posterior results.

Appendix S1. Cryptotephra extraction methods.

Figure S1. Location of total cryptotephra sample columns at Arma Veirana.

Acknowledgements. This research would not have been possible without the help of various researchers, funding organizations and students. We gratefully acknowledge Harangi Szabolcs from Eötvös University for helpful guidance as well as Chris Campisano, Michael Barton, John Murray, B. Patrick Fahey and Andrew Zipkin from Arizona State University for helping improve this manuscript. Field-work at RB and AV is made possible by ongoing collaborations with and administrative support from the *Soprintendenza Archaeologia, Belle Arti e Paesaggio per la città metropolitana di Genova e Le province di Imperia, La Spezia e Savona*, the *Polo Museale della Liguria*, and the Museo Preistorico Nazionale dei Balzi Rossi, and the priceless logistical support from the Istituto Internazionale di Studi Liguri. We also would like to acknowledge Daniella Gandolfi in Bordighera for the RB project as well as the ProLoco of Erli and the town of Cerisola for the AV project. We acknowledge funding from the following agencies and organizations: National Science Foundation (BCS-1917173 and BCS-1460366 to E.I.S. and BCS-1917191 and BCS-1460376 to C.W.M.); Hyde Family Foundations; the Institute of Human Origins (IHO) at Arizona State University (ASU); the John Templeton Foundation to the IHO at ASU; the Office of Knowledge Enterprise Development, Graduate Professional and Student Association (GPSA), and the Graduate College at ASU; National Geographic (Waitt Program W391-15); Social Sciences and Humanities Research Council of Canada (#435-2017-1520 and #430-2018-00846); the H2020 European Research Council (n.724046 – SUCCESS); Fonds de Recherche du Québec-Société et Culture (2016-NP-193048); the Canada Foundation for Innovation (JFELS Grant #37754); the Université de Montréal; the Wenner-Gren Foundation; the Leakey Foundation; CU Denver ORS, CRISP; Washington University in St. Louis; and the Cryptotephra Laboratory for Archaeological and Geological Research (CLAGR) at the University of Nevada, Las Vegas (UNLV). The opinions expressed in this publication are those of the author(s) and do not necessarily reflect the views of any of these funding organizations. All authors and co-authors declare no conflict of interest.

Abbreviations. AV, Arma Veirana; BM, Black Mousterian; CI, Campanian Ignimbrite; CSB, Compact Strong Brown; Gr, Granular; HREE, heavy rare earth elements; LREE, light rare earth elements; MCMC, Markov chain Monte Carlo; MIS, Marine Isotope Stage; NP- MANOVA, non-parametric analysis of variance; RB, Riparo Bombrini.

References

- Abbott PM, Austin WEN, Davies SM, *et al.* 2014. Re-evaluation and extension of the Marine Isotope Stage 5 tephrostratigraphy of the Faroe Islands region: the cryptotephra record. *Palaeogeography, Palaeoclimatology, Palaeoecology* 409: 153–168, <https://doi.org/10.1016/j.palaeo.2014.05.004>
- Aksu AE, Jenner G, Hiscott RN, *et al.* 2008. Occurrence, stratigraphy and geochemistry of Late Quaternary tephra layers in the Aegean Sea and the Marmara Sea. *Marine Geology* 252: 174–192, <https://doi.org/10.1016/j.margeo.2008.04.004>
- Albert PG, Tomlinson EL, Smith VC, *et al.* 2017. Glass geochemistry of pyroclastic deposits from the aeolian Islands in the last 50 ka: a proximal database for tephrochronology. *Journal of Volcanology and Geothermal Research* 336: 81–107, <https://doi.org/10.1016/j.jvolgeores.2017.02.008>
- Barton RNE, Lane CS, Albert PG, *et al.* 2015. The role of cryptotephra in refining the chronology of Late Pleistocene human evolution and cultural change in North Africa. *Quaternary Science Reviews* 118: 151–169, <https://doi.org/10.1016/j.quascirev.2014.09.008>
- Benazzi S, Slon V, Talamo S, *et al.* 2015. The makers of the Protoaurignacian and implications for Neandertal extinction. *Science* 348: 793–796, <https://doi.org/10.1126/science.aaa2773>
- Blockley SPE, Pyne-O'Donnell SDF, Lowe JJ, *et al.* 2005. A new and less destructive laboratory procedure for the physical separation of distal glass tephra shards from sediments. *Quaternary Science Reviews* 24: 1952–1960, <https://doi.org/10.1016/j.quascirev.2004.12.008>

- Bronk Ramsey C. 2013. OxCal version 4.2.2. University of Oxford Radiocarbon Accelerator Unit. Computer Program. Available at: c14.arch.ox.ac.uk/embed.php?File=oxcal.html
- Brown F, Harris J, Leakey R, *et al.* 1985. Early *Homo erectus* skeleton from west Lake Turkana, Kenya. *Nature* 316: 788–792, <https://doi.org/10.1038/316788a0>
- Cauche D. 2007. Les cultures moustériennes en Ligurie italienne: analyse du matériel lithique de trois sites en grotte. *L'Anthropologie* 111: 254–289, <https://doi.org/10.1016/j.anthro.2007.05.002>
- Cauche D, Tozzi C, Vicino G, *et al.* 2002. L'Exploitation différentielle des matières premières lithiques par les moustériens dans deux sites de Ligurie (Italie). *Pierre et Archeologie* 177–193.
- Chiarabba C., De Gori P., Speranza F. 2008. The southern Tyrrhenian subduction zone: Deep geometry, magmatism and Plio-Pleistocene evolution. *Earth and Planetary Science Letters* 268(3–4): 408–423. [10.1016/j.epsl.2008.01.036](https://doi.org/10.1016/j.epsl.2008.01.036)
- Christiansen EH, Haapala I, Hart GL. 2007. Are Cenozoic topaz rhyolites the erupted equivalents of Proterozoic rapakivi granites? Examples from the western United States and Finland. *Lithos* 97: 219–246, <https://doi.org/10.1016/j.lithos.2007.01.010>
- Douka K, Jacobs Z, Lane C, *et al.* 2014. The chronostratigraphy of the Haua Fteah cave (Cyrenaica, northeast Libya). *Journal of Human Evolution* 66: 39–63, <https://doi.org/10.1016/j.jhevol.2013.10.001>
- Douka K, Grimaldi S, Boschian G, *et al.* 2012. A new chronostratigraphic framework for the Upper Palaeolithic of Riparo Mochi (Italy). *Journal of Human Evolution* 62: 286–299, <https://doi.org/10.1016/j.jhevol.2011.11.009>
- Druitt TH, Brenchley PJ, Gökten YE, *et al.* 1995. Late Quaternary rhyolitic eruptions from the Acigöl Complex, central Turkey. *Journal of the Geological Society* 152: 655–667, <https://doi.org/10.1144/gsjgs.152.4.0655>
- Ellis AR, Burchett WW, Harrar SW, *et al.* 2017. Nonparametric inference for multivariate data: the R package nrmv. *Journal of Statistical Software* 76: 1–18.
- Ewart A. 1963. Petrology and petrogenesis of the Quaternary pumice ash in the Taupo area, New Zealand. *Journal of Petrology* 4: 392–431, <https://doi.org/10.1093/petrology/4.3.392>
- Feibel CS. 1999. Tephrostratigraphy and geological context in paleoanthropology. *Evolutionary Anthropology* 8: 87–100. [https://doi.org/10.1002/\(SICI\)1520-6505\(1999\)8:33.0.CO;2-W](https://doi.org/10.1002/(SICI)1520-6505(1999)8:33.0.CO;2-W)
- Feibel CS, Brown FH, McDougall I. 1989. Stratigraphic context of fossil hominids from the Omo group deposits: northern Turkana Basin, Kenya and Ethiopia. *American Journal of Physical Anthropology* 78: 595–622, <https://doi.org/10.1002/ajpa.1330780412>
- Forni F, Lucchi F, Peccerillo A, *et al.* 2013. Stratigraphy and geological evolution of the Lipari volcanic complex (central Aeolian archipelago), *Geological Society, London, Memoirs* 213–279, <https://doi.org/10.1144/M37.10>
- Gehrels MJ, Lowe DJ, Hazell ZJ, *et al.* 2006. A continuous 5300-yr Holocene cryptotephrostratigraphic record from northern New Zealand and implications for tephrochronology and volcanic hazard assessment. *Holocene* 16: 173–187, <https://doi.org/10.1191/0959683606hl918rp>
- Gelman A, *et al.* 2013. *Bayesian Data Analysis*. Chapman & Hall/CRC: New York.
- Harris JA, Marean CW, Ogle K, *et al.* 2017. The trajectory of bone surface modification studies in paleoanthropology and a new Bayesian solution to the identification controversy. *Journal of Human Evolution* 110: 69–81, <https://doi.org/10.1016/j.jhevol.2017.06.011>
- Higham T. 2011. European middle and upper Palaeolithic radiocarbon dates are often older than they look: problems with previous dates and some remedies. *Antiquity* 85: 235–249, <https://doi.org/10.1017/S0003598X00067570>
- Higham T, Brock F, Peresani M, *et al.* 2009. Problems with radiocarbon dating the Middle to Upper Palaeolithic transition in Italy. *Quaternary Science Reviews* 28: 1257–1267, <https://doi.org/10.1016/j.quascirev.2008.12.018>
- Higham T, Douka K, Wood R, *et al.* 2014. The timing and spatiotemporal patterning of Neanderthal disappearance. *Nature* 512: 306–309, <https://doi.org/10.1038/nature13621>
- Holt B, Negrino F, Riel-Salvatore J, *et al.* 2019. The Middle–Upper Paleolithic transition in Northwest Italy: new evidence from Riparo Bombrini (Balzi Rossi, Liguria, Italy). *Quaternary International* 508: 142–152, <https://doi.org/10.1016/j.quaint.2018.11.032>
- Insinga DD, Tamburrino S, Lirer F, *et al.* 2014. Tephrochronology of the astronomically-tuned KC01B deep-sea core, Ionian Sea: insights into the explosive activity of the Central Mediterranean area during the last 200 ka. *Quaternary Science Reviews* 85: 63–84, <https://doi.org/10.1016/j.quascirev.2013.11.019>
- Jakobsson SP, Jónasson K, Sigurdsson IA. 2008. The three igneous rock series of Iceland. *Jökull* 58: 117–138.
- Jónasson K. 2007. Silicic volcanism in Iceland: composition and distribution within the active volcanic zones. *Journal of Geodynamics* 43: 101–117, <https://doi.org/10.1016/j.jog.2006.09.004>
- Jowitt SM, Medlin CC, Cas RAF. 2017. The rare earth element (REE) mineralisation potential of highly fractionated rhyolites: a potential low-grade, bulk tonnage source of critical metals. *Ore Geology Reviews* 86: 548–562, <https://doi.org/10.1016/j.oregeorev.2017.02.027>
- Koutrouli A, Anastakis G, Kontakiotis G, *et al.* 2018. The early to mid-Holocene marine tephrostratigraphic record in the Nisyros–Yali-Kos volcanic center, SE Aegean Sea. *Journal of Volcanology and Geothermal Research* 366: 96–111, <https://doi.org/10.1016/j.jvolgeores.2018.10.004>
- Kuehn SC, Froese DG, Shane PAR. 2011. The INTAV intercomparison of electron-beam microanalysis of glass by tephrochronology laboratories: results and recommendations. *Quaternary International* 246: 19–47, <https://doi.org/10.1016/j.quaint.2011.08.022>
- Kuhn SL, Stiner MC. 1998. The Earliest Aurignacian of Riparo Mochi (Liguria, Italy). *Current Anthropology* 39: 175–189, <https://doi.org/10.1086/204694>
- Lane CS, Cullen VL, White D, *et al.* 2014. Cryptotephra as a dating and correlation tool in archeology. *Journal of Archeological Science* 42: 42–50, <https://doi.org/10.1016/j.jas.2013.10.033>
- Lowe DJ. 1990. Tephra studies in New Zealand: an historical review. *Journal of the Royal Society of New Zealand* 20: 119–150, <https://doi.org/10.1080/03036758.1990.10426736>
- Lowe DJ. 2011. Tephrochronology and its application: a review. *Quaternary Geochronology* 6: 107–153, <https://doi.org/10.1016/j.quageo.2010.08.003>
- Lowe JJ, Ramsey CB, Housley RA, *et al.* 2015. The RESET project: constructing a European tephra lattice for refined synchronisation of environmental and archaeological events during the last c. 100 ka. *Quaternary Science Reviews* 118: 1–17, <https://doi.org/10.1016/j.quascirev.2015.04.006>
- Lunn D, Spiegelhalter D, Thomas A, *et al.* 2009. The BUGS project: evolution, critique and future directions. *Statistics in Medicine* 28: 3049–3067, <https://doi.org/10.1002/sim.3680>
- Martin E, Sigmundsson O. 2007. Crustal thermal state and origin of silicic magma in Iceland: the case of Torfajökull, Ljósufjöll and Snæfellsjökull volcanoes. *Contributions to Mineralogy and Petrology* 153: 593–605, <https://doi.org/10.1007/s00410-006-0165-5>
- Matthews IP, Trincardi F, Lowe JJ, *et al.* 2015. Developing a robust tephrochronological framework for Late Quaternary marine records in the southern Adriatic Sea: new data from core station SA03-11. *Quaternary Science Reviews* 118: 84–104, <https://doi.org/10.1016/j.quascirev.2014.10.009>
- Miller CF, Mittlefehldt DW. 1982. Depletion of light rare-earth elements in felsic magmas. *Geology* 10: 129–133, [DOI: 10.1130/0091-7613(1982)10<129:DOLREI>2.0.CO;2].
- Negrino F, Arobba D, Conventi M, *et al.* 2018. L'Arma degli Zerbi (Finale Ligure, SV): un sito riscoperto. In *Preistoria and Protostoria Della Liguria*, Negrino F, Tiné VIstituto Internazionale di Preistoria e Protostoria: Florence; 87.
- Paterne M, Guichard F, Labeyrie J. 1988. Explosive activity of the South Italian volcanoes during the past 80,000 years as determined by marine tephrochronology. *Journal of Volcanology and Geothermal Research* 34: 153–172, [https://doi.org/10.1016/0377-0273\(88\)90030-3](https://doi.org/10.1016/0377-0273(88)90030-3)
- Peccerillo A. 2005. *Plio-Quaternary Volcanism in Italy: Petrology, Geochemistry, Geodynamics*. Springer: Berlin.
- R Development Core Team, RFFSC. 2017. *R: A Language and Environment for Statistical Computing*. R Foundation for Statistical Computing: Vienna.

- Reimer PJ, Bard E, Bayliss A, *et al.* 2013. IntCal13 and Marine13 radiocarbon age calibration curves 0–50,000 years cal bp. *Radiocarbon* 55: 1869–1887, https://doi.org/10.2458/azu_js_rc.55.16947
- Riede F, Thastrup MB. 2013. Tephra, tephrochronology and archeology – a (re-)view from northern Europe. *Heritage Science* 1: 1–17, <https://doi.org/10.1186/2050-7445-1-15>
- Riel-Salvatore J, Ludeke IC, Negrino F, *et al.* 2013. A spatial analysis of the Late Mousterian Levels of Riparo Bombrini (Balzi Rossi, Italy). *Canadian Journal of Archeology* 37: 70–92.
- Riel-Salvatore J, Negrino F. 2018a. Human adaptations to climatic change in Liguria across the Middle-Upper Paleolithic transition. *Journal of Quaternary Science* 33: 313–322, <https://doi.org/10.1002/jqs.3005>
- Riel-Salvatore J, Negrino F. 2018b). Proto-Aurignacian lithic technology, mobility, and human niche construction: a case study from Riparo Bombrini, Italy. In *Lithic Technological Organization and Paleoenvironmental Change*: 163–187. Springer International.
- Rivière É. 1887. Paléolithologie: de l'antiquité de l'homme dans les Alpes-Maritimes. JB Baillière.
- Ruffini R, Cadoppi P, D'Atri A. 1995). Ash layers in the Monferrato (NW Italy): records of two types of magmatic source in Oligocene–Miocene time
- Ash layers in the Monferrato (NW Italy): records of two types of magmatic source in Oligocene–Miocene time. *Eclogae Geologicae Helveticae* 88/2: 347–363.
- Sarna-Wojcicki AM, Meyer CE, Bowman HR, *et al.* 1985. Correlation of the Rockland Ash Bed, a 400,000-year-old stratigraphic marker in northern California and western Nevada, and implications for Middle Pleistocene paleogeography of central California. *Quaternary Research* 23: 236–257, [https://doi.org/10.1016/0033-5894\(85\)90031-6](https://doi.org/10.1016/0033-5894(85)90031-6)
- Satow C, Tomlinson EL, Grant KM, *et al.* 2015. A new contribution to the Late Quaternary tephrostratigraphy of the Mediterranean: Aegean Sea core LC21. *Quaternary Science Reviews* 117: 96–112, <https://doi.org/10.1016/j.quascirev.2015.04.005>
- Seghedi I, Helvacı C. 2016. Early Miocene Kirka-Phrigian Caldera, western Turkey (Eskişehir province), preliminary volcanology, age and geochemistry data. *Journal of Volcanology and Geothermal Research* 327: 503–519, <https://doi.org/10.1016/j.jvolgeores.2016.09.007>
- Shane P, Hovard J. 2002. Distal record of multi-sourced tephra in Onepoto Basin, Auckland, New Zealand: implications for volcanic chronology, frequency and hazards. *Bulletin of Volcanology* 64: 441–454, <https://doi.org/10.1007/s00445-002-0217-2>
- Siebel W, Schmitt AK, Kiemele E, *et al.* 2011. Acigöl rhyolite field, central Anatolia (part II): geochemical and isotopic (Sr-Nd-Pb, $\delta^{18}\text{O}$) constraints on volcanism involving two high-silica rhyolite suites. *Contributions to Mineralogy and Petrology* 162: 1233–1247, <https://doi.org/10.1007/s00410-011-0651-2>
- Smith EL, Jacobs Z, Johnsen R, *et al.* 2018. Humans thrived in South Africa through the Toba eruption about 74,000 years ago. *Nature* 555: 511–515, <https://doi.org/10.1038/nature25967>
- Sun S-s, McDonough WF. 1989. Chemical and isotopic systematics of oceanic basalts: implications for mantle composition and processes, *Geological Society, London, Special Publications* 313–345, <https://doi.org/10.1144/GSL.SP.1989.042.01.19>
- Tomlinson EL, Kinvig HS, Smith VC, *et al.* 2012. The Upper and Lower Nisyros Pumices: revisions to the Mediterranean tephrostratigraphic record based on micron-beam glass geochemistry. *Journal of Volcanology and Geothermal Research* 243–244: 69–80, <https://doi.org/10.1016/j.jvolgeores.2012.07.004>
- Tomlinson EL, Smith VC, Albert PG, *et al.* 2015. The major and trace element glass compositions of the productive Mediterranean volcanic sources: tools for correlating distal tephra layers in and around Europe. *Quaternary Science Reviews* 118: 48–66, <https://doi.org/10.1016/j.quascirev.2014.10.028>
- Tomlinson E. L., Thordarson T., Müller W., *et al.* 2010. Microanalysis of tephra by LA-ICP-MS - Strategies, advantages and limitations assessed using the Thorsmörk ignimbrite (Southern Iceland), *Chemical Geology. Elsevier B.V.* 279(3–4): 73–89. [10.1016/j.chemgeo.2010.09.013](https://doi.org/10.1016/j.chemgeo.2010.09.013).
- Tryon CA, Kuhn SL, Slimak L, *et al.* 2011. Scale in tephrostratigraphic correlation: an example from Turkish Pleistocene archeological sites. *Quaternary International* 246: 124–133, <https://doi.org/10.1016/j.quaint.2011.05.039>
- Tryon CA, Logan MAV, Mouralis D, *et al.* 2009. Building a tephrostratigraphic framework for the Paleolithic of Central Anatolia, Turkey. *Journal of Archeological Science* 36: 637–652, <https://doi.org/10.1016/j.jas.2008.10.006>
- Veres D, Cosac M, Schmidt C, *et al.* 2018. New chronological constraints for Middle Palaeolithic (MIS 6/5–3) cave sequences in Eastern Transylvania, Romania. *Quaternary International* 485: 103–114, <https://doi.org/10.1016/j.quaint.2017.07.015>
- Vicino G. 1984. Lo scavo paleolitico al Riparo Bombrini (Balzi Rossi di Grimaldi, Ventimiglia). *Riv Ing Int* 39: 1–10.
- De Vivo B., *et al.* 2001. New constraints on the pyroclastic eruptive history of the Campanian volcanic Plain (Italy). *Mineralogy and Petrology* 73(1-3): 47–65. [10.1007/s007100170010](https://doi.org/10.1007/s007100170010).
- Wagner B, Sulpizio R, Zanchetta G, *et al.* 2008. The last 40 ka tephrostratigraphic record of Lake Ohrid, Albania and Macedonia: a very distal archive for ash dispersal from Italian volcanoes. *Journal of Volcanology and Geothermal Research* 177: 71–80, <https://doi.org/10.1016/j.jvolgeores.2007.08.018>
- White WM. 2013. *Geochemistry*. John Wiley & Sons, Ltd: Chichester.
- Wulf S, Kraml M, Brauer A, *et al.* 2004. Tephrochronology of the 100ka lacustrine sediment record of Lago Grande di Monticchio (southern Italy). *Quaternary International* 122: 7–30, <https://doi.org/10.1016/j.quaint.2004.01.028>